AIAA JOURNAL
Vol. 40, No. 11, November 2002

Planar Blast/Vortex Interaction and Sound Generation

H. Chen* and S. M. Liang†
National Cheng-Kung University, Tainan 701, Taiwan, Republic of China

By the use of a fifth-order weighted essentially nonoscillatory scheme to solve the two-dimensional, unsteady compressible Euler equations, a planar blast/vortex interaction is investigated in detail. The effects of the initial blast Mach number M_S and vortex Mach number M_V are discussed and compared with the corresponding cases of shock/vortex interaction. The sound generated by the planar blast/vortex interaction is also studied. It is found that the radial pressure peaks of the first sound for the cases of shock/vortex interaction are larger than those for the cases of blast/vortex interaction. However, the radial pressure peaks of the second sound in the blast/vortex interaction can be larger than those in the corresponding case of shock/vortex interaction. This is due to the effect of the secondary shock interacting with the vortex, enhanced by the expansion waves following the blast-wave front. In addition, an interesting phenomenon of the fourth sound, which is an exception from the first three sounds generated by the blast/vortex interaction, is found that does not occur in the case of a shock/vortex interaction.

I. Introduction

BLAST waves are generated by the collapse of high-pressure gas containers, the detonation of solid explosives, laser beam focusing in ambient air, and nuclear explosions. Recently, there have been many studies related to blast waves, but very few dealt with the problem of blast/vortex interaction. A blast wave is much closer to a practical case, such as compression waves coalescing into a weak shock in the exhaust gas pipes of automobile engines. The interaction of a shock wave with a vortex is well known to be one of the major sources of noise and is closely related to some aerodynamic problems, such as the noises produced by rockets, high-speed aircraft, and helicopters. Because of the expansion waves accompanying the shock front of a blast wave, the phenomenon of blast/vortex interaction is very complicated and may be similar to that of shock/vortex interaction. Thus, the basic mechanisms of the shock-wave/vortex interaction help in understanding the blast/vortex interaction.

Hollingsworth and Richards[1] showed experimentally that when a columnar vortex passed through a planar shock wave, a cylindrical acoustic wave appeared with a portion cut off by the shock wave. They observed that the acoustic wave consisted of alternating compressions and rarefactions (quadrupolar nature). Dosanjh and Weeks[2] verified experimentally the quadrupolar nature in a shock tube by using an airfoil at an angle of attack to generate a starting vortex. Ribner[3] decomposed the vortex by a Fourier transform into planar sinusoidal shear waves in a radial symmetric fashion. The planar sound waves produced by each shear/shock interaction were recombined in a Fourier integral. The wave possessed an envelope that was essentially a growing cylindrical sound wave centered at the transmitted vortex. The pressure jump (Ribner referred to the first sound as a precursor) across the nominal radius, $r = R$ ($R = ct$) is attenuated with time as $R^{-1/2}$ and varied around this circle in an antisymmetric fashion, except for a portion cut off by the shock wave resembling a quadrupolar field, where c denotes the speed of sound downstream of the shock wave. Good agreement was obtained except near the shock. The pressure jump decayed like R^{-1}. Later, Ribner compared his updated approximate result with an experimental result and found that both results were fairly similar but had a relative shift. This is because the theoretical description for a vortex is exactly antisymmetric, but the experimental vortex is not. Ellzey et al.[4] simulated the shock/vortex interaction problem by using the Euler equations. Their numerical results compared well with the theoretical result of Ribner[3] and the experimental result of Dosanjh and Weeks.[2] They pointed out that the strengths of both a shock wave and a vortex can greatly affect the flow structure induced by the shock/vortex interaction. A strong shock wave can result in a Mach reflection and a weak shock wave generates a regular reflection. They also showed that both the precursor (first sound) and the second sound are of quadrupolar nature. Subsequently, Ellzey and Henneke[5] studied the issue of the origin of acoustic noise in shock-wave/vortex interactions and showed that shock distortion and vortex deformation were responsible for the development of the acoustic field.

Because direct numerical simulation of the far-field sound has been feasible in recent years, Inoue and Hattori[6] studied the detailed mechanics of the flowfield produced by the interactions between a single vortex or a pair of vortices and a shock wave by using the Navier–Stokes equations. They first explored the basic nature of the sound pressure field for the case of a single vortex and then for a vortex pair. In their study, the effect of the Reynolds number seemed insignificant. Inoue[7] examined the propagation process of the sound waves from the near to the far field and confirmed the existence of the third sound wave. Grasso and Pirozzoli[8] studied the interaction of a shock wave with a cylindrical vortex by means of a weighted essentially nonoscillatory (WENO) scheme. They investigated the effects of the vortex intensity and shock strength and determined the dependence of shock distortion and vortex compression, as well as subsequent nutation, on the shock and vortex strength.

The objective of this paper is to analyze planar blast/vortex interaction with emphasis on the flowfield and the mechanism of sound production using a high-resolution Euler solver. The numerical method was developed by means of a fifth-order WENO scheme of Jiang and Shu.[9] We will pay attention to the flow structure induced by the secondary shock, which may also produce sound in addition to the sounds generated by shock/vortex interaction. In addition to blast/vortex interactions, shock/vortex interactions with the same conditions are also simulated for comparison.

II. Description of Physical Problem and Numerical Method

A schematic for a vortex and a rectangular region of high-pressure air with thickness x_0 used to generate a planar blast wave is shown in Fig. 1. The planar blast wave is produced by rupture of the high-pressure region. The vortex, with its center located at the origin, rotates in a counterclockwise direction. The planar blast wave moves from left to right with respect to the vortex. A polar coordinate system (r, θ) used for the vortex is also shown in Fig. 1. The vortex formulation used in this study is the same as that of Inoue and Hattori,[6] and the distance between the vortex center and the high-pressure region is chosen to be x_e. In our simulation, all boundary conditions imposed are the nonreflecting conditions of Thompson.[10,11]

Received 24 July 2001; revision received 28 May 2002; accepted for publication 11 July 2002.

*Graduate Student, Institute of Aeronautics and Astronautics.
†Professor, Institute of Aeronautics and Astronautics. Associate Fellow AIAA.

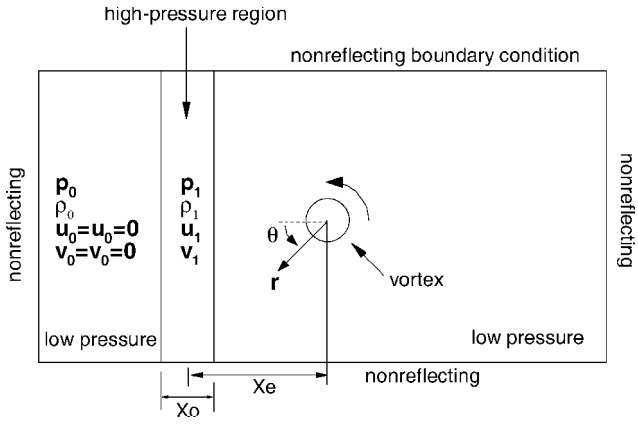

Fig. 1 Schematic diagram of flow model with initial and boundary conditions.

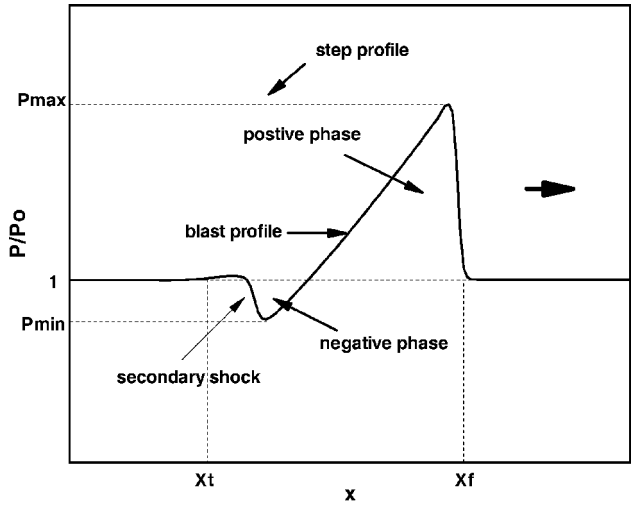

Fig. 2 Typical pressure distribution for a blast wave.

Assume the airflow is inviscid. The governing equations are the two-dimensional, time-dependent Euler equations, which can be written in a conservation form. A high-order numerical method is developed for solving the Euler equations. For spatial derivatives, the fifth-order WENO scheme of Jiang and Shu[9] is adopted, and a fourth-order Runge–Kutta method is used for time integration. Because the blast-wave intensity decays with time at $t = 0$, the blast-wave front starts interaction with the vortex at $x = -2$. For the comparison of the blast and shock/vortex interactions, the values of Mach number for both cases are chosen to be the same. The vortex Mach number defined as $M_V = (u_\theta)_{\max}/c_0$, where $(u_\theta)_{\max}$ denotes the maximum tangential velocity and c_0 denotes the sound speed of the undisturbed air.

A typical characteristic of a blast wave due to the rapid release of energy in a gas is shown in Fig. 2. The major difference between a planar shock wave and a planar blast wave is that the flow properties behind the shock-wave front are constant. However, behind the blast-wave front, there is a blast profile region in which the flow properties are rapidly decreased due to expansion waves. Because the blast-wave intensity decays with time, the range $(x_t \le x \le x_f)$ of the blast-wave profile will be increased, and the magnitudes of $P_{\max}$ and $P_{\min}$ of the blast wave will be decreased. The Courant–Friedrichs–Lewy number (CFL) is chosen to be CFL = 0.6. The minimum local time step over the computational domain is chosen for all unsteady-flow calculations. The computational domain is $\{(x, y)|-15 \le x \le 15, -15 \le y \le 15\}$ and a uniform grid with $\Delta x = \Delta y = 0.05$ is used to ensure that the WENO scheme is of fifth-order accuracy in space.

III. Results and Discussion

A. Basic Flow Structure of Blast/Vortex Interaction

The basic flow structure caused by the blast/vortex interaction is shown schematically in Fig. 3. Figure 3a shows the blast-wave front

Table 1 Parameters of blast wave, vortex, and initial conditions

Case	M_S	M_V	p_1/p_0	x_0	x_e
A	1.05	0.25	1.74	0.2	8
B	1.05	0.5	1.74	0.2	8
C	1.2	0.25	8.0	0.2	10
D	1.2	0.5	8.0	0.2	10

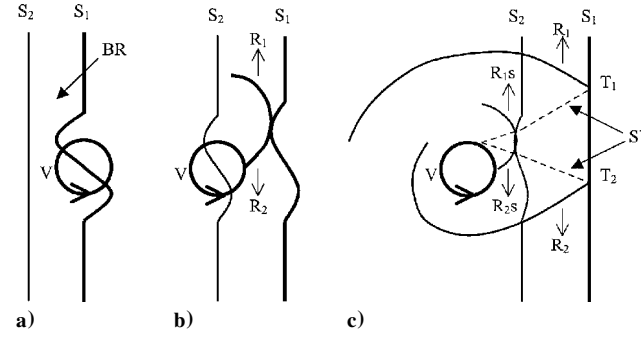

Fig. 3 Process of blast-wave/vortex interaction at different instants: a) blast-wave front interacting with vortex, b) secondary shock wave S_2 interacting with vortex, V and c) the blast wave (S_1 and S_2) after passing through the vortex V.

S_1, deformed because of vortex influence. As time increases, the planar blast wave is further deformed; two reflected shock waves, R_1 and R_2, emanating from a high-pressure compression region develop; and the secondary shock S_2 interacts with the vortex, as shown in Fig. 3b. The secondary shock is also deformed in its shape. Later, the blast-wave front and the secondary shock will pass through the vortex. For weak blast waves and weak vortices, two regular reflections and two slip lines (SL) can occur, as shown in Fig. 3c. The reflected shock waves, SL, and blast-wave front intersect at the two triple points, $T1$ and $T2$. For strong blast waves and strong vortices, two Mach reflections may occur instead of regular reflections.

In this study, the Mach numbers M_S of the blast-wave front chosen for starting interaction with the vortex were 1.05 and 1.2. The vortex Mach number, representing the vortex strength, was chosen to be 0.25 or 0.5. The values of the parameters used for the blast/vortex interaction from case A to case D are listed in Table 1. Cases A and B denote weak blast waves interacting with a vortex. Cases C and D denote stronger blast waves interacting with a vortex.

It was found that there is no Mach reflection associated with the secondary shock in our simulation. The reason is that the blast waves were too weak to form a Mach reflection. Our simulation result for case C is shown in Figs. 4a–4f. These results are computational shadowgraphs of blast/vortex interaction at different instants from $t = 2$–12 with an increment of $\Delta t = 2$. Note that in all of our simulations, the beginning of the blast wave or shock wave to interact with a vortex is set to $t = 0$. In Fig. 4, all of the reflected shocks, triple points, and SL are clearly shown. These flow structures have been described in Fig. 3. In Fig. 4a, the blast-wave front S_1 is interacting with the vortex V. In Fig. 4b, the blast-wave front is deformed, and the reflected shock waves start to from the blast-wave front. In Fig. 4c, the secondary shock S_2 is interacting with the vortex. The blast-wave front S_1 becomes almost straight. The reflected shock waves R_1 and R_2 and the SL are clearly shown in Fig. 4c. The reflected shock R_1 intersects the secondary shock, but R_2 does not. In Figs. 4d and 4e, the secondary shock interacting with the vortex results in additional reflected shock waves (R_1s and R_2s). In Fig. 4f, the blast/vortex interaction is finished. The blast-wave front almost resumes its straight shape. When the vortex Mach number is increased, the reflected shock waves R_1, R_2, R_1s, and R_2s will be more deformed, much like a spiral pattern as shown in Fig. 3c. If there were no accompanying secondary shock and its associated reflected shock waves, the flowfield would be similar to that for a shock/vortex interaction.

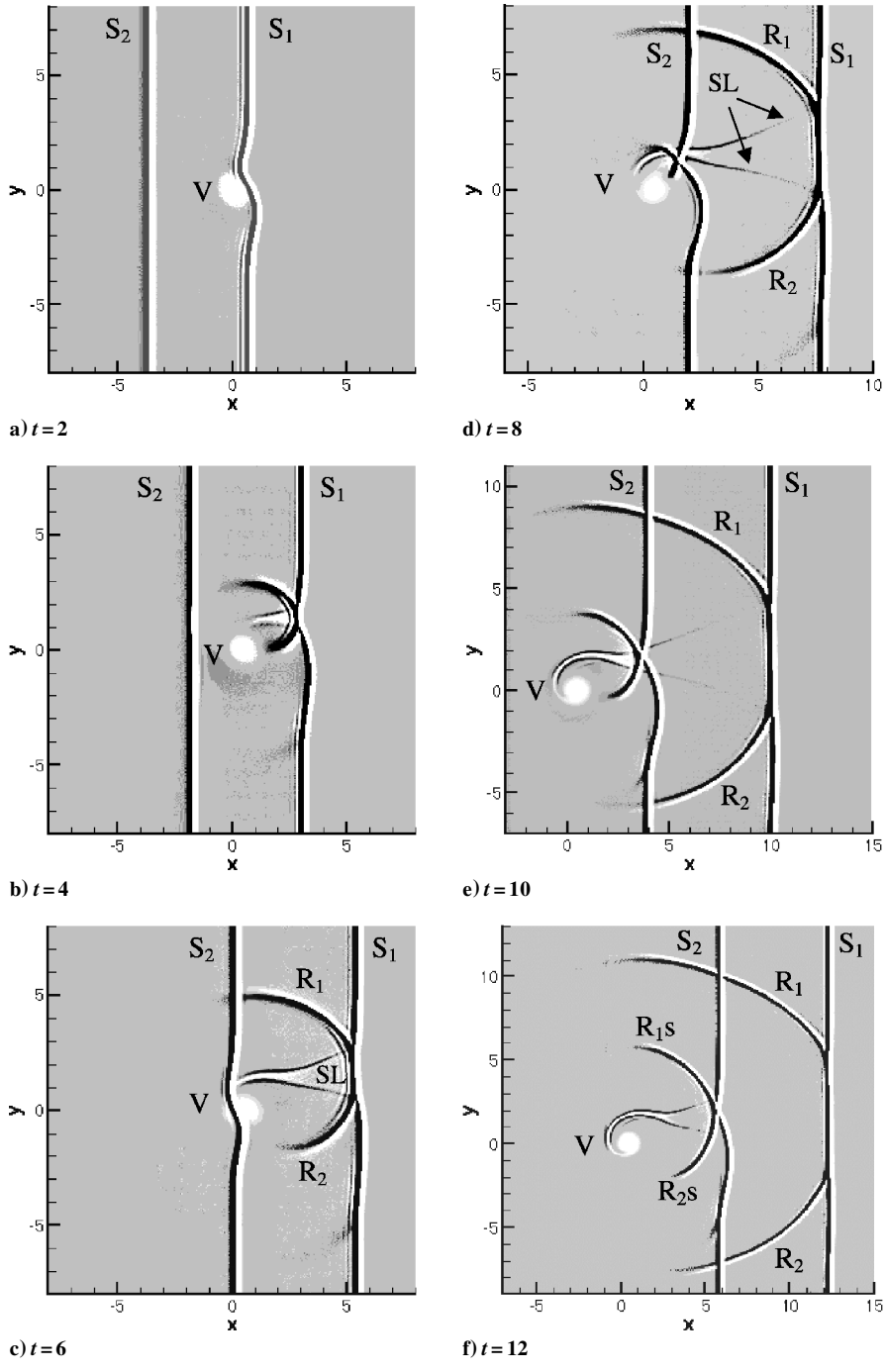

Fig. 4 Computational shadowgraphs for blast wave/vortex interaction at different instants.

B. Sound Generation by Blast/Vortex Interaction

Up to now, there are very few reports about the blast/vortex interaction, neither computations nor experiments, for our comparison. To verify the reliability and accuracy of our computational results, we compared our results with the experimental data of Dosanjh and Weeks,[2] the theoretical result of Ribner,[3] and the computational results of Ellzey et al.[4] and of Inoue and Hattori.[6] Our numerical simulations were performed by setting $M_S = 1.29$ and $M_V = 0.39$, the experimental condition used by Dosanjh and Weeks.[2] Figure 5 shows the comparison of the circumferential distributions of the pressure amplitude, which is defined as $(p_2 - p_p)/p_s$, where the symbol p_p denotes the peak pressure of the precursor, p_2 the peak pressure of the second sound, and p_s the pressure behind the shock wave. In the experiment of Dosanjh and Weeks,[2] an interferogram was taken when the radius of the "acoustic wave" was approximately 10 times that of the vortex core. In our simulation, the flowfield at the radius of the acoustic wave (about 10 times that of the vortex core) was evaluated approximately at $t = 10.3$, as referred to by Inoue and Hattori.[6] As seen from Fig. 5, the present result is very close to both the computational results of Inoue and Hattori[6] and of Ellzey et al.[4] This shows that the present solver is able to compute the flowfields induced by the shock or blast/vortex interactions accurately. The experimental result in Fig. 5 seems to have a little shift in contrast to other results. The reason is that the theoretical description for a vortex is exactly antisymmetric. The formulation for a vortex in numerical simulation is also "perfect," but the experimental one is not. The density and sound pressure [defined as $\Delta p = (p - p_s)/p_s$] fields obtained at the conditions as in the experiment of Dosanjh and Weeks[2] are almost the same as those obtained by Inoue and Hattori.[6] Therefore, these results are not presented here.

The sound generation by blast/vortex interaction is more complicated than that due to shock/vortex interaction because of the effects

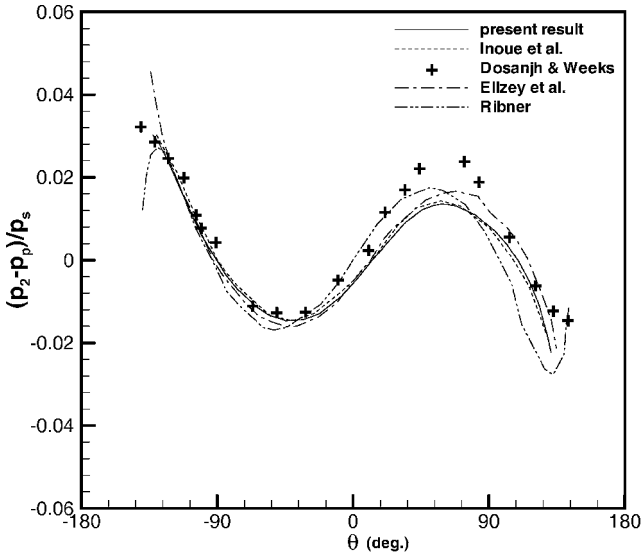

Fig. 5 Comparison of the present Euler result with the experimental data of Dosanjh and Weeks,[2] the theory of Ribner,[3] the Euler result of Ellzey et al.,[4] and the Navier–Stokes result of Inoue and Hattori[6] for shock/vortex interactoin.

of the decaying blast-wave strength, blast profile region, and secondary shock. The sound pressure of planar blast/vortex interaction is defined as $\Delta p = (p - p_0)/p_0$, where p_0 denotes the reference pressure as shown in Fig. 1. A sequence of the sound pressure fields of case A listed in Table 1 is presented in Fig. 6. Figure 6a shows the beginning of the blast-wave/vortex interaction. At the early stage of the interaction, the sound generated due to the blast-wave front distortion shows a dipolar character, as shown in Fig. 6b. Later, it changes to a quadrupolarone, as shown in Figs. 6c and 6d. In contrast to the case of shock/vortex interaction, we find a rarefaction region following the reflected shocks R_1 and R_2. The rarefaction may be caused by the expansion waves in the blast profile. Moreover, the sound pressure field profiles of the upper and lower regions near the blast-wave front have a sawtooth shape, which are quite different from those in the corresponding shock/vortex interaction. As seen from Fig. 6, the entire sound pressure fields are similar to those for the shock/vortex interaction. With the blast Mach number or vortex Mach number increasing, the entire flowfield becomes very complicated because of the stronger interactions caused by the strong blast, expansion waves, secondary shock, and vortex. However, the basic nature of a quadrupolar phenomenon was still found to exist. The pressure peaks of the precursor and second sound wave generated at $\theta = -45$ deg for the four cases in Table 1 are plotted against the radial distance r, as shown in Figs. 7 and 8. The differences of the peak sound pressures between the fine and coarse

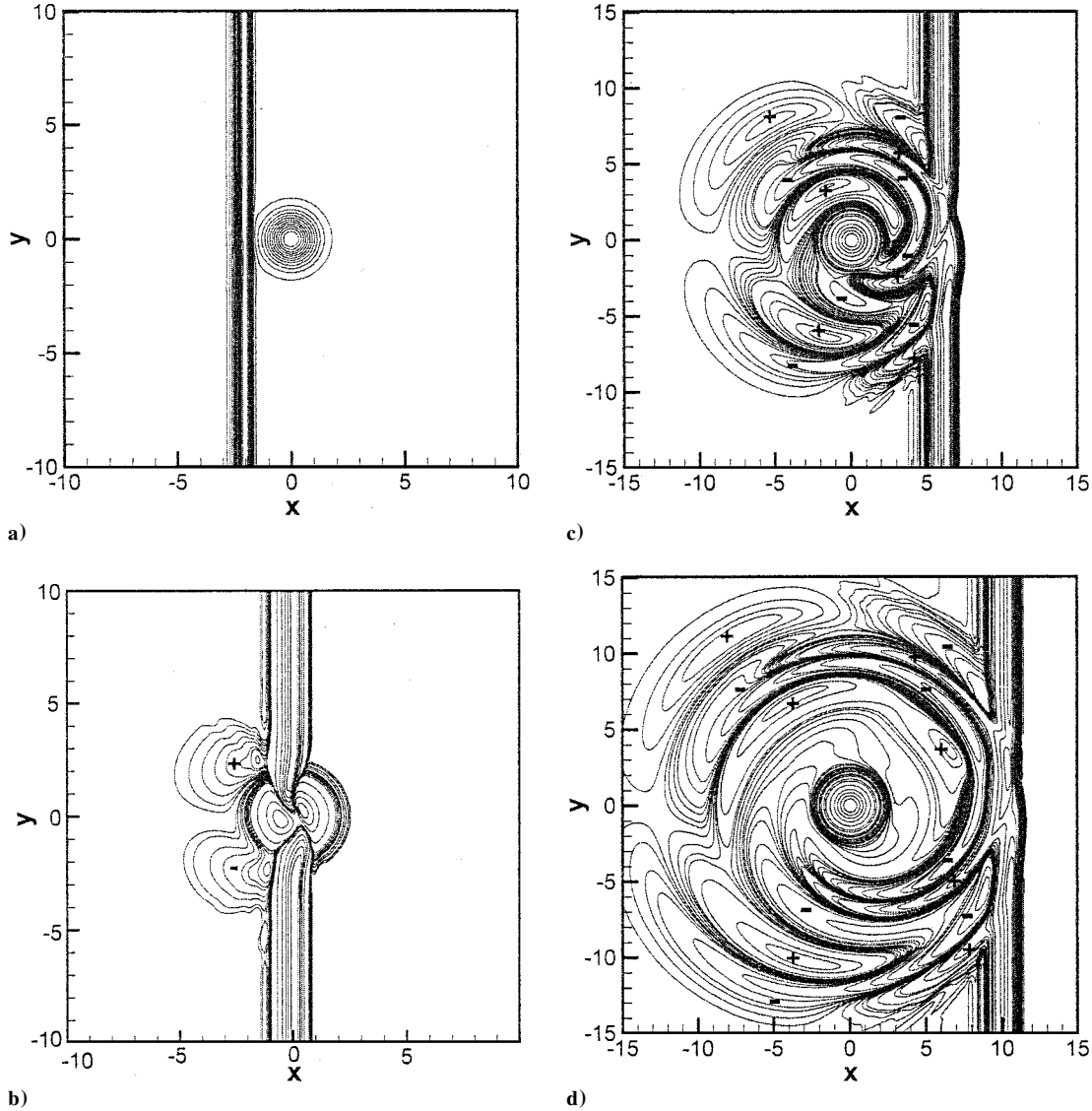

Fig. 6 Sound pressure Δp contours at different instants: a) $t = 0$, b) $t = 2$, c) $t = 8$, and d) $t = 12$; +, the compression region and −, the rarefaction region.

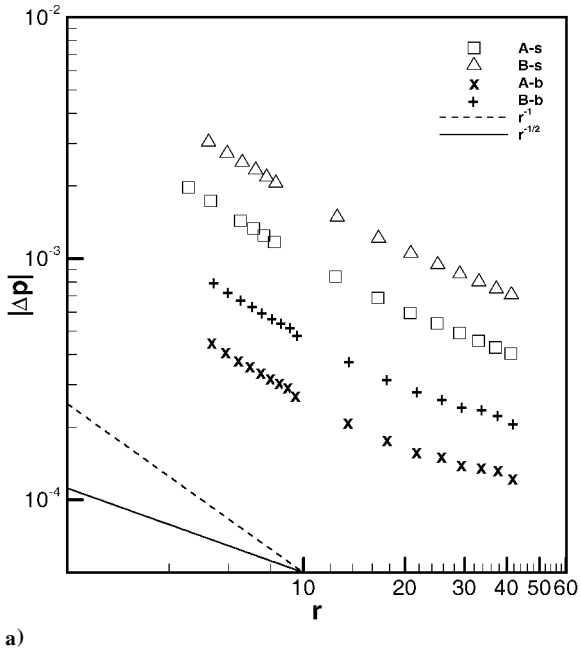

a)

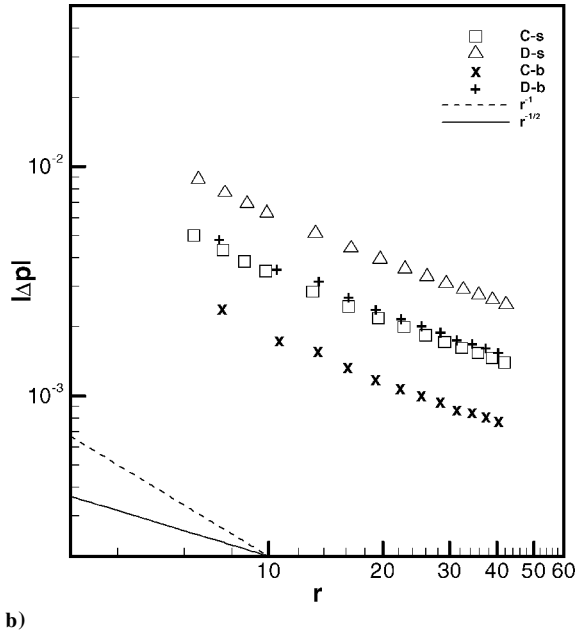

b)

Fig. 7 Pressure peaks of the first sound vs the radial distance r at $\theta = -45$ deg; A-s denotes case A of shock/vortex interaction, A-b case A of blast/vortex interaction, etc., for a) weak shock and blast waves (cases A and B) and b) stronger shock and blast waves (cases C and D).

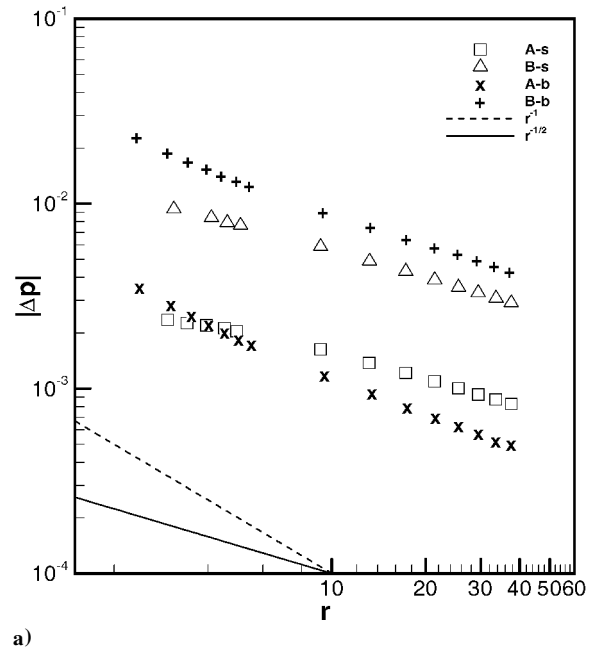

a)

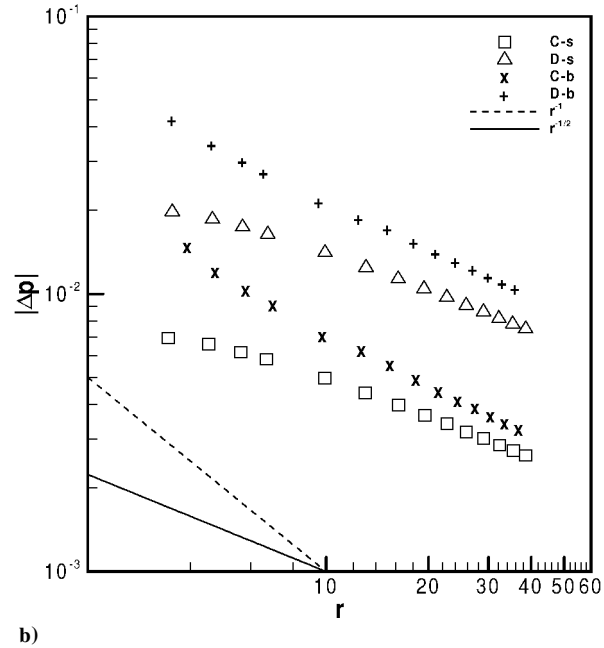

b)

Fig. 8 Pressure peaks of the second sound vs the radial distance r at $\theta = -45$ deg; C-s denotes case C of shock/vortex interaction, etc., for a) weak shock and blast waves (cases A and B) and b) stronger shock and blast waves (cases C and D).

grids are negligibly small, as mentioned by Inoue and Hattori.[6] To save the computational time and computer memory, the computational domain $\{(x, y)|-45 \le x \le 45, -45 \le y \le 45\}$ and a uniform grid with spacing $x = \Delta y = 0.1$ were adopted to simulate the sound generation process in the far field. Note that, in Figs. 7 and 8, the results of shock/vortex interaction are included and compared with those for the corresponding blast/vortex interactions. The notation A-s in Figs. 7 and 8 denotes case A in the problem of shock/vortex interaction, and notation A-b case A for the problem of blast/vortex interaction. Other notations such as B-s, C-b, etc., are easily understood. As seen from Figs. 7a and 7b, for all cases, the pressure peaks of the precursor tend to decay like r^{-1} in the near field ($r < 10$) and $r^{-1/2}$ in the far field ($r > 10$). Obviously, our results agree well with the theory. Figure 7a shows that the pressure peaks of the first sound for the shock/vortex interaction (SVI) case are larger than those for the blast/vortex interaction (BVI) case. This is because stronger interaction occurs in the shock-wave case compared with the corresponding BVI, in which the blast-wave strength is decaying during propagation. Figure 7b shows that the radial pressure peaks in the stronger shock- and blast-wave cases. One can see that the pressure peaks (denoted by +) for the D-b case are larger than those (denoted by □) for the C-s case. Namely, a stronger vortex with a weak blast wave can produce an interaction that is stronger than that for the case of a stronger shock with a weak vortex.

Figure 8 shows the decay of pressure peaks of the second sound for cases A–D. One can clearly see that the pressure peaks for the B-b and D-b cases are larger than those for other three cases, as shown in Figs. 8a and 8b, respectively. This means that a stronger blast wave interacting with a stronger vortex can produce a strong second sound. Thus, the vortex strength is equally important as the shock or blast strength, and their interaction is mutual. In particular, unlike the A-b case as shown in Fig. 8a, the pressure peaks (×) of the second sound in the C-b case are larger than those (□) in the case of the C-s case. It is conjectured that this difference is caused by the second shock interacting with the vortex, enhanced by stronger expansion waves following the stronger blast-wave front. As for the radial decay of the second sound, from Fig. 8 one can see that for the

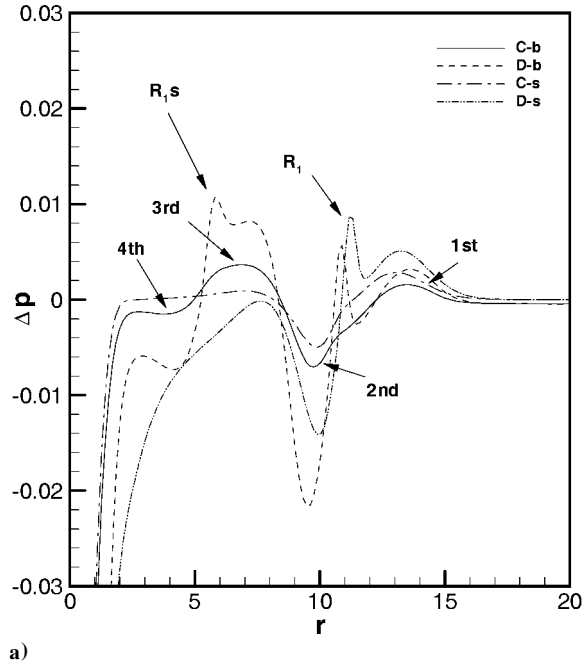

a)

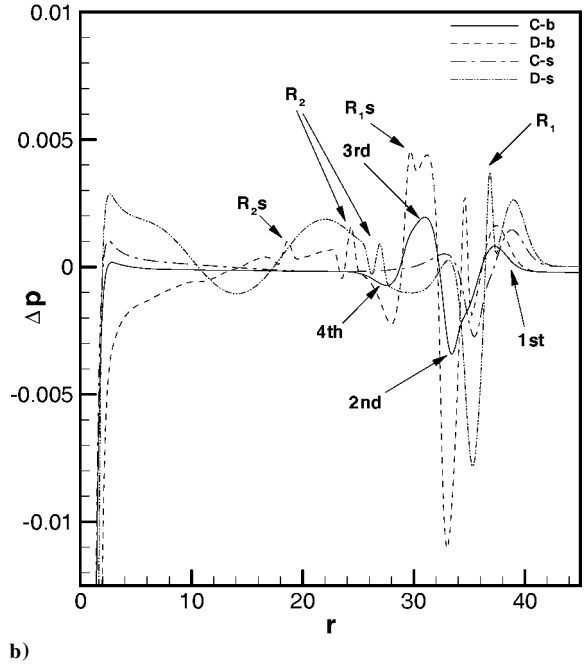

b)

Fig. 9 Radial distribution of sound pressure at a) $t = 12$ and b) $t = 36$; C-b denotes case C of blast/vortex interaction, etc.

blast-wave cases the pressure peaks apparently tend to decay faster than for the shock-wave cases, especially in the near field; however, it seems to decay like $r^{-1/2}$ in the far field. The verification requires a much larger domain and is left for future work. Figure 9 shows the radial distribution of sound pressure for cases C and D at $t = 12$ and 36 and at $\theta = -45$ deg. In Fig. 9a, the peak pressure magnitudes of the second sound for the blast wave cases are apparently larger than that for the corresponding shock-wave cases. The reason is due to the expansion waves/vortex interaction for the blast-wave case. The reflected shock waves R_1 only occur in the stronger vortex strength cases ($M_V = 0.5$) because the vortex Mach number effect causes the reflected shock waves to deform. In Fig. 9b, the vortex Mach number effect is clearly shown, especially in the transition region, that is, the region behind the fourth sound for the blast-wave case, or the third sound for the shock-wave case. The vortex Mach number can influence the reflected shock, peak sound pressure level, and the transition regions where both effects of the vortex strength and lower reflected shock waves are strong. In addition, we found that

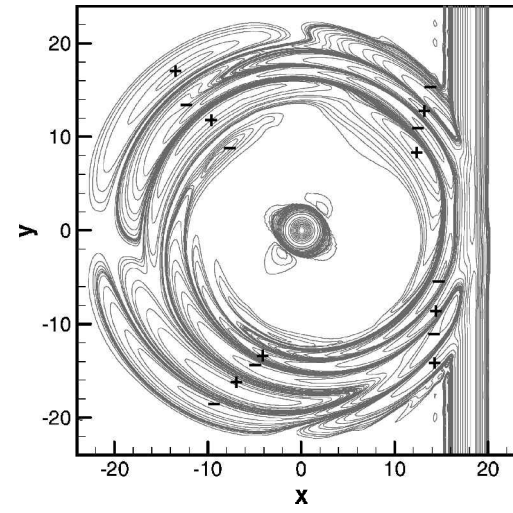

Fig. 10 Appearance of the fourth sound occurred in blast/vortex interaction at $t = 20$ (case A).

the positions of the peak sound pressure such as the precursor and second sound are not changed if the blast or shock Mach number is kept the same. Figure 9 also shows evidence for the existence of the fourth sound generated by the planar BVI in comparison with the corresponding planar SVI. The sound pressure field of case A at $t = 20$ is shown in Fig. 10. It is clearly shown that the fourth sound is of quadrupolar nature. We tried to increase the time domain from $t_{\max} = 40$ to 48 to see whether more sounds are generated. However, only four sounds were observed in our case. This may be because the BVI in the present study is not strong enough to generate more than four sounds. This problem requires further investigation of very strong BVI.

IV. Conclusions

By the use of a fifth-order WENO scheme to solve the two-dimensional, unsteady compressible Euler equations, the flowfields of a planar BVI were studied in detail. The effects of the initial blast Mach number M_S and vortex Mach number M_V were discussed and compared with the corresponding cases of SVI. The present results show that large values of M_S or M_V produce strong compressions and rarefactions and that weak blast waves result in regular reflections associated with the blast-wave front, whereas strong blast waves result in Mach reflections. The sound generated by the planar BVI is of quadrupolar nature, as in an SVI. The precursor generated by the BVI tends to decay like r^{-1} in the near field and $r^{-1/2}$ in the far field as in the corresponding SVI. The radial pressure peaks of the first sound for the SVI cases are larger than those for the BVI cases. As for the second sound, it decays faster than that for the SVI. However, it seems to decay like $r^{-1/2}$ in the far field. Moreover, the pressure peaks of the second sound in the BVI can be larger than those in the corresponding case of SVI. This is due to the interaction of the secondary shock with the enhanced vortex by the expansion waves following the blast-wave front. The fourth sound generated by a planar BVI is found to exist in the present study but not in the case of an SVI.

Acknowledgments

The support of this work under contract with the National Science Council, NSC 90-2213-E006-096, is gratefully acknowledged. The authors thank M. Platzer and K. Jansma for reading the manuscript. The authors also thank the reviewers for their valuable comments and suggestions.

References

[1]Hollingsworth, M. A., and Richards, E. J., "A Schlieren Study of the Interaction Between a Vortex and a Shock Wave in a Shock Tube," Aeronautical Research Council Fluid Motion Subcommittee, Rept. ARC 17985, FM 2323, London, 1955.

[2]Dosanjh, D. S., and Weeks, T. M., "Interaction of a Starting Vortex as Well as a Vortex Street with a Traveling Shock Wave," *AIAA Journal*, Vol. 3, No. 2, 1965, pp. 216–223.

[3]Ribner, H. S., "Cylindrical Sound Wave Generated by a Ring Vortex–Shock Wave Interaction," *AIAA Journal*, Vol. 23, No. 11, 1985, pp. 1708–1715.

[4]Ellzey, J. L., Henneke, M. R., Picone, J. M., and Oran, E. S., "The Interaction of a Shock with a Vortex: Shock Distortion and the Production of Acoustic Waves," *Physics of Fluids*, Vol. 7, No. 1, 1995, pp. 172–184.

[5]Ellzey, J. L., and Henneke, M. R., "The Shock–Vortex Interaction: the Origins of the Acoustic Wave," *Fluid Dynamics Research*, Vol. 21, No. 3, 1997, pp. 171–184.

[6]Inoue, O., and Hattori, Y., "Sound Generation by Shock–Vortex Interactions," *Journal of Fluid Mechanics*, Vol. 380, Feb. 1999, pp. 81–116.

[7]Inoue, O., "Propagation of Sound Generated by Weak Shock–Vortex Interaction," *Physics of Fluids*, Vol. 12, No. 5, 2000, pp. 1258–1261.

[8]Grasso, F., and Pirozzoli, S., "Shock-Wave–Vortex Interactions: Shock and Vortex Deformations, and Sound Production," *Theoretical and Computational Fluid Dynamics*, Vol. 13, No. 6, 2000, pp. 421–456.

[9]Jiang, G.-S., and Shu, C.-W., "Efficient Implementation of Weighted ENO Schemes," *Journal of Computational Physics*, Vol. 126, No. 1, 1996, pp. 202–228.

[10]Thompson, W., "Time Dependent Boundary Conditions for Hyperbolic Systems," *Journal of Computational Physics*, Vol. 68, No. 1, 1987, pp. 1–24.

[11]Thompson, W., "Time Dependent Boundary Conditions for Hyperbolic Systems II," *Journal of Computational Physics*, Vol. 89, No. 2, 1990, pp. 439–461.

M. Sichel
Associate Editor